Chemistry
A European
Journal

Chemistry Europe
European Chemical Societies Publishing

Accepted Article

Title: In cellulo generation of fluorescent probes for live-cell imaging of cylooxygenase-2

Authors: Jatinder Kaur, Atul Bhardwaj, and Frank Wuest

To be cited as: *Chem. Eur. J.* 10.1002/chem.202003315

Link to VoR: https://doi.org/10.1002/chem.202003315

WILEY-VCH

10.1002/chem.202003315

WILEY-VCH

FULL PAPER

In cellulo generation of fluorescent probes for live-cell imaging of cylooxygenase-2

Jatinder Kaur[a],[b] †, Atul Bhardwaj[a],[b] †, and Frank Wuest [a],[b],[c] *

[a] Department of Oncology,
University of Alberta,
Edmonton, AB, Canada
[b] Faculty of Pharmacy and Pharmaceutical Sciences,
University of Alberta,
Edmonton, AB, Canada
[c] Department of Chemistry,
University of Alberta,
Edmonton, AB, Canada

† Authors contributed equally to this work
* Corresponding author (wuest@ualberta.ca)

Supporting information for this article is given via a link at the end of the document.

Keywords: Cyclooxygenase-2, Fluorogenic click chemistry, Live cell imaging.

Abstract: Live-cell imaging with fluorescent probes is an essential tool in chemical biology to visualize the dynamics of biological processes in real-time. Intracellular disease biomarker imaging remains a formidable challenge due to the intrinsic limitations of conventional fluorescent probes and the complex nature of cells. Here, we describe the *in cellulo* assembly of a fluorescent probe to image cyclooxygenase-2 (COX-2). We developed celecoxib-azide derivative **14**, possessing favorable biophysical properties and excellent COX-2 selectivity profile. *In cellulo* strain-promoted fluorogenic click chemistry of COX-2-engaged compound **14** with non/weakly-fluorescent compounds **11** and **17** formed fluorescent probes **15** and **18** for the detection of COX-2 in living cells. Competitive binding studies, biophysical, and comprehensive computational analyses were used to describe protein-ligand interactions. The reported new chemical toolbox enables precise visualization and tracking of COX-2 in live cells with superior sensitivity in the visible range.

Introduction

Molecular imaging is a powerful technology in chemical biology and clinical research to decipher the molecular basis of diseases and aid the development of novel diagnostic and therapeutic tools to enhance patient care.[1-3] Fluorescence imaging enables real-time and high-resolution visualization of disease biomarkers in their cellular environment. However, the development of small-molecule fluorescent imaging probes for targeting intracellular biomarkers remains challenging due to background noise, and the potential loss of potency and specificity due to the incorporation of rather large fluorescent tags. Assembly and activation of fluorescent probes upon binding to their molecular target within living cells represent an innovative and exciting strategy to overcome these intrinsic limitations. Intracellular assembly and activation of small-molecule fluorescent probes enable the imaging of biomarkers in living cells with high specificity and sensitivity. Cyclooxygenase-2 (COX-2) enzyme is a crucial inducible biomarker in many inflammatory diseases, including cancer.[4-6] In contrast to constitutively expressed COX-1 isoform, COX-2 is highly overexpressed and activated under acute and chronic inflammatory conditions. High COX-2 levels are also present in several types of cancer, such as colorectal, stomach, breast, lung and prostate cancers.[4-9]

Many nonsteroidal anti-inflammatory drugs (NSAIDs), including selective COX-2 inhibitors like celecoxib **1**, have been tested in clinical trials as promising chemoprevention and anticancer drugs. Anticancer activity of NSAIDs is linked mainly to the suppression of COX-2-mediated biosynthesis of prostaglandin E_2 (PGE_2).[9-12] COX-2 also converts various pro-carcinogens into carcinogens through its peroxidase activity which promotes tumor growth, inhibits apoptosis and contributes to angiogenesis, tumor invasion, and metastasis.[4]

The design of cell-permeable, highly potent and specific COX-2 imaging probes represents a formidable challenge to unfold further the role of COX-2 in cancer and other diseases at the cellular and molecular level. However, to date, only a few COX-2 imaging probes have been reported.[13-19] Marnett *et al.* have recently developed Fluorocoxib A, a fluorescent probe based on non-selective COX inhibitor indomethacin.[13] At the cellular level, COX-2 resides primarily in the nuclear envelope and endoplasmic reticulum region. Crystallography data suggest that the COX-2 active site is embedded deeply in the enzyme structure and accessible through an L-shaped channel (molecular lobby).[20,21] Therefore, COX-2 fluorescent imaging probes should possess favorable physicochemical properties to cross cellular membranes and enter the molecular lobby to bind to the COX-2 active site with high affinity and selectivity.

Synthesis of fluorescent imaging probes usually involves the incorporation of a fluorogenic tag into the periphery of an intact targeting molecule. This strategy often compromises the favorable pharmacological properties of the targeting molecule resulting in weaker potency and reduced specificity. Alternatively, we envisioned a different design strategy where a highly potent and target-specific fluorescent imaging probe is generated through fluorogenic click chemistry upon binding to COX-2 in living cells. This approach involves specific binding of a non-fluorescent molecule to COX-2 followed by *in cellulo* fluorogenic click chemistry with another non/weakly-fluorescent compound to generate a highly fluorescent "turn-on" imaging probe within the COX-2 active site. Click chemistry has attracted massive attention in chemical biology, material sciences and biomedical research due to their fascinating efficiency, versatility, high reaction rates, and biocompatibility.[22-27] The prototype reaction involves the Cu(I)-catalysed [3+2] cycloaddition between azides and alkynes (CuAAC), but especially strain-promoted Cu-free click chemistry has found numerous applications in chemical and biological sciences.[28-32] Prominent examples include kinetic target-guided synthesis[33-37], protein modification and profiling[38-41], labeling of glycans[42-45], proteins,[46-50] lipids[51, 52], nucleic acid[53-55], and other biomolecules.[56,67] Herein, we describe the first example of using fluorogenic strain-promoted click chemistry for real-time visualization of COX-2 in living cells with superior sensitivity in the visible range.

10.1002/chem.202003315

Results and Discussion

Rational design

Anti-inflammatory drug celecoxib (compound **1**) was selected as a suitable chemical template for the design of COX-2 targeting fluorescent imaging probes.[11,58] Our design strategy (Figure S1) considered that *i)* the target-engaged compound (celecoxib-alkyne/azide) displays high affinity and selectivity for COX-2, *ii)* COX-2 binding and complementary non/weakly-fluorescent compound possess good cell permeability profile and stability in biological fluids, *iii)* both compounds undergo rapid fluorogenic click chemistry in living cells, and *iv)* the corresponding product is strongly fluorescent.

We first designed a virtual library of COX-2 binding compounds consisting of celecoxib analogs decorated with clickable functional groups and linkers through comprehensive computational analyses (Table S1, S2). After assessing their binding mode to COX-2 and synthetic accessibility, we selected celecoxib analogs **3**, **9,** and **14** as promising COX-2 binding compounds for click chemistry in living cells (Figure 1).

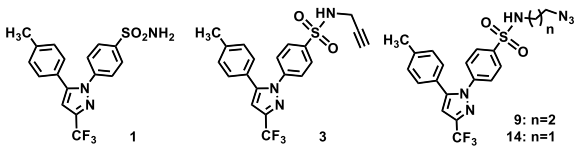

Figure 1. Structure of celecoxib **1** and COX-2 binding compounds **3**, **9** and **14**.

Compounds **3**, **9**, and **14** occupied favorable conformations within the COX-2 active site as indicated by interactions with critical amino acid residues R120, S353, and Y355, whereas no significant interactions were with COX-1 isoform. Inhibition of constitutively expressed COX-1 is not desirable, as it is involved in the biosynthesis of essential prostaglandins to maintain homeostasis.[59] Interestingly, molecular docking and molecular dynamic (MD) simulation studies also revealed that the azide group in compound **14** is not buried inside the COX-2 active site but reaching out of the COX-2 active site. This molecular orientation makes the azide group in compound **14** particularly easily accessible for subsequent click chemistry reactions (Figures S2-S4).

Chemistry

The results of our computational analysis prompted us to set up the synthesis of celecoxib analogs containing a terminal alkyne (compound **3**) or an azide group (compounds **9** and **14**) for subsequent click chemistry with respective azides or alkynes (Scheme S1).

Compound **3** was reacted with 3-azido-7-diethylamino-chromen-2-one **4** (Scheme S2) to give celecoxib-coumarin **5** in 82.5% yield. However, celecoxib-coumarin **5** was found not suitable for cell imaging studies due to rapid photobleaching and unfavorable fluorescence properties (λ_{ex} = 347 nm, λ_{em} = 430 nm), which are in the same range as the autofluorescence signal of the used COX-2 expressing colorectal cancer HCA-7 cells. Therefore, we coupled celecoxib-alkyne **3** with 4-azido-7-nitro-benzo[1,2,5]oxa-diazole (NBD-azide) **6** (Scheme S3) to yield triazole **7** in 84.5% yield. However, NBD-azide **6** was itself highly fluorescent, and upon CuAAC reaction with celecoxib-alkyne **3** the resulting triazole compound **7** displayed weak fluorescence. Thus, celecoxib-alkyne **3** was found not suitable for *in cellulo* click chemistry with either coumarin-azide **4** or with NBD-azide **6**. Alternatively, we prepared a new series of COX-2 binding azides (compounds **9** and **14**) as well as alkyne compound **11** as complementary click chemistry building blocks. Click chemistry products **12** and **15** were obtained in isolated 85.0 and 88.5% yield, respectively, using typical CuAAC reaction conditions (Scheme 1). Both compounds differ in the carbon chain linker length separating the fluorescent tag from the COX-2 binding celecoxib scaffold.

Compound **14** containing a two-carbon chain linker displayed more favorable COX-2 inhibitory potency and selectivity compared to three-carbon chain analog **9** (Table 1), and therefore compound **14** was selected for further studies.

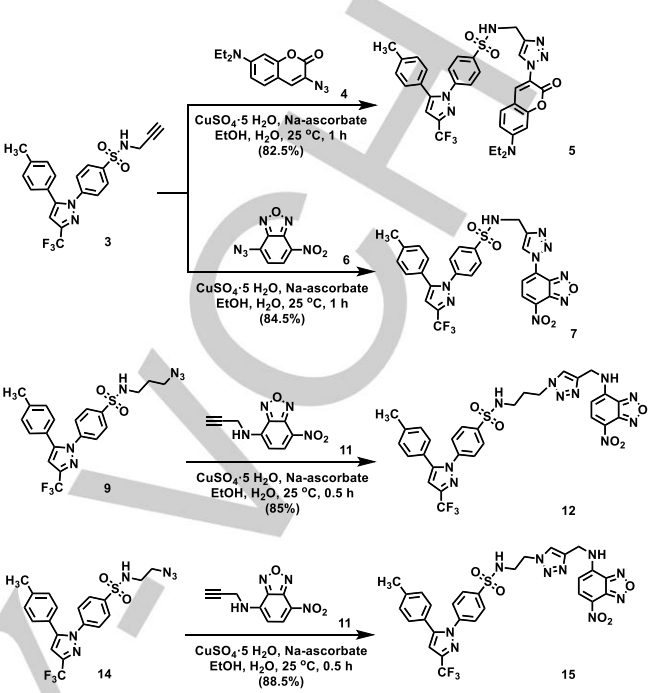

Scheme 1. Synthesis of compounds **5**, **7**, **12**, and **15**.

Compounds **14** and **11** showed weak fluorescence signal, while CuAAC product celecoxib-triazole-NBD **15** was highly fluorescent (λ_{em} = 537 nm, Φ_F = 0.78, 1% DMSO in PBS) and photostable. By comparing the structures of compounds **3**, **6** and **7** with compounds **14**, **11** and **15**, respectively, we noticed the importance of the carbon chain length (two *versus* three) and the functional group (azide *versus* alkyne) in the COX-2 binding celecoxib analogs on the resulting fluorescence properties of the CuAAC product. Fluorescence properties differed significantly, and compounds **14** and **11** were further studied as suitable candidates for the development of fluorescent imaging probes for live-cell imaging of COX-2.

In order to use celecoxib-azide **14** for Cu-free strain-promoted click chemistry in living cells, we prepared dibenzocyclooctyne-NBD (NBD-DBCO) compound **17**. Reaction of commercially available 4-chloro-7-nitrobenzo[c][1,2,5]oxadiazole **10** with DBCO-amine **16** afforded compound **17** in 88% yield. Subsequent strain-promoted click chemistry of **17** with celecoxib-azide **14** gave fluorescent compound **18** in 85% isolated yield. (Scheme 2).

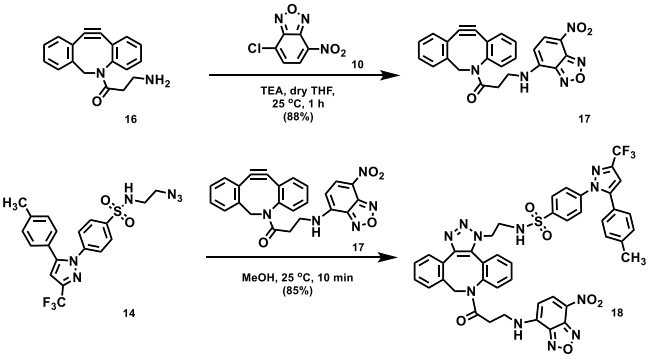

Scheme 2. Synthesis of DBCO compound **17** and fluorescent celecoxib derivative **18**.

DBCO-based compounds are highly popular as versatile building blocks for Cu-free click chemistry in living biological systems. Feasibility of strain-promoted click chemistry between celecoxib-azide **14** and NBD-DBCO **17** to form fluorescent compound **18** was tested before its use in living cells. Absorption and fluorescence emission data revealed that both compounds **14** and **17** are weakly-fluorescent whereas click chemistry product **18** is strongly fluorescent (λ_{em} = 539 nm, Φ_F = 0.79, 1% DMSO in PBS). The significant differences in fluorescence between click chemistry building block **14** and **17**, and click chemistry product **18** make the proposed strategy highly suitable for the development of an *"off-on"* COX-2 responsive fluorescence imaging probe in living cells.

COX-1 and COX-2 inhibition and selectivity studies

Celecoxib analogs **3**, **9** and **14** and respective click chemistry products **5**, **7**, **12**, **15** and **18** were evaluated for *in vitro* COX-1 and COX-2 inhibitory and selectivity profiles along with important physicochemical properties like lipophilicity (log*P*) and polar surface area (PSA) (Table 1). *In cellulo* COX-2 inhibitory activities were determined in COX-2-expressing HCA-7 cells.

Table 1. COX-1 and COX-2 inhibition data, COX-2 selectivity index (SI), and calculated logP and PSA data of compounds **1, 3, 5, 7, 9, 12, 14, 15** and **18**.

Compd.	IC_{50} COX-1 (μM)	IC_{50} COX-2 (μM)	COX-2 SI	Cellular IC_{50} (μM)	log $P_{o/w}$	PSA
1	>100	0.05	>2000	0.09	3.34	80.86
3	88.6	0.49	180.8	0.91	4.29	66.49
5	>100	1.12	>90.9	2.65	6.27	140.79
7	91.6	0.78	117.4	0.98	3.07	182.86
9	>100	0.11	>900	0.78	3.63	115.59
12	97.8	0.49	199.6	0.97	4.33	201.53
14	>100	0.023	>4350	0.08	3.16	118.84
15	>100	0.054	>1850	0.21	3.47	197.59
18	>100	0.12	>830	0.89	7.32	218.15

IC_{50}, half-maximal inhibitory concentration; SI, COX-2 selectivity index: [(COX-1 IC_{50})/(COX-2 IC_{50})]; Compounds tested in COX-2 overexpressing HCA-7 cells; data represented as mean values of three determinations. The octanol/water partition coefficient (log $P_{O/W}$) and van der Waals surface area of N and O atoms and carbonyl C atoms (PSA) were calculated using QikProp.

Celecoxib-alkyne **3** showed selective COX-2 inhibition (IC_{50} = 0.49 μM), representing an almost 10-fold decrease of inhibitory potency compared to celecoxib **1** (IC_{50}= 0.054 μM). Notably, lead compound celecoxib-azide **14** displayed high COX-2 inhibtion activity, Notably, lead compound celecoxib-azide **14** displayed high COX-2 inhibitory activity (IC_{50} = 0.023 µM), which was in the same range as celecoxib **1** (IC50 = 0.054 µM). The high COX-2 selectivity over COX-1 inhibitory activity (COX-2 SI >4300) of celecoxib-azide **14** further supports its use as a suitable COX-2 binding compound and its transformation into fluorescent COX-2 imaging probes in living cells. After testing click chemistry products **5**, **7**, **12**, **15** and **18** for their COX-1 and COX-2 inhibition, celecoxib-T-NBD **15** (IC_{50} = 0.054 μM) and compound **18** (IC_{50} = 0.12 μM) showed favorable COX-2 inhibitory potency and selectivity profiles. We also calculated several important drug descriptors linked to ADME properties (Table S3). Lead compound celecoxib-azide **14** displayed a favorable octanol/water partition coefficient (log $P_{O/W}$ = 3.63), Caco-2 cell permeability (mimic of gut-blood barrier (QP P_{Caco}=151.82 nm/sec), MDCK cell permeability (mimic of blood-brain barrier, QP P_{MDCK} = 310.67 nm/sec), and a suitable ADME profile (Table S3). Moreover, the high COX-2 inhibitory potency and selectivity profile of compound **14** further support the use of celecoxib-azide **14** as a suitable COX-2 targeting compound in living cells.

Chemical stability of compound 11, 14, 15, 17 and 18

Chemical stability and photostability of compounds **11, 14, 15, 17,** and **18** were assessed in PBS (pH 7.4), human and rat serum through monitoring fluorescence emission and LC-MS analysis over time. All compounds displayed a suitable stability profile for over six hours (Figure 2). Additionally, no significant changes of native fluorescence in PBS, DMEM, FBS, human serum, rat serum, cell lysate as well as in the presence or absence of detergents such as Triton X-100 and Tween-20 at 37 °C further confirmed the suitability of compounds **11, 14, 15, 17** and **18** for biological labeling experiments (Figure S5).

Fluorescence-based thermal shift assay (TSA) was used for assessing protein-ligand interactions of celecoxib-azide **14** and compounds **15** and **18** with COX-2 and COX-1. Incubation of celecoxib azide **14** with recombinant human COX-2 protein resulted in a positive melting temperature shift (ΔT_M = 9.2 °C), indicating that binding of compound **14** to COX-2 resulted in a noticeable thermal stabilization of the COX-2 protein compared to the unbound state (Figure 2d).

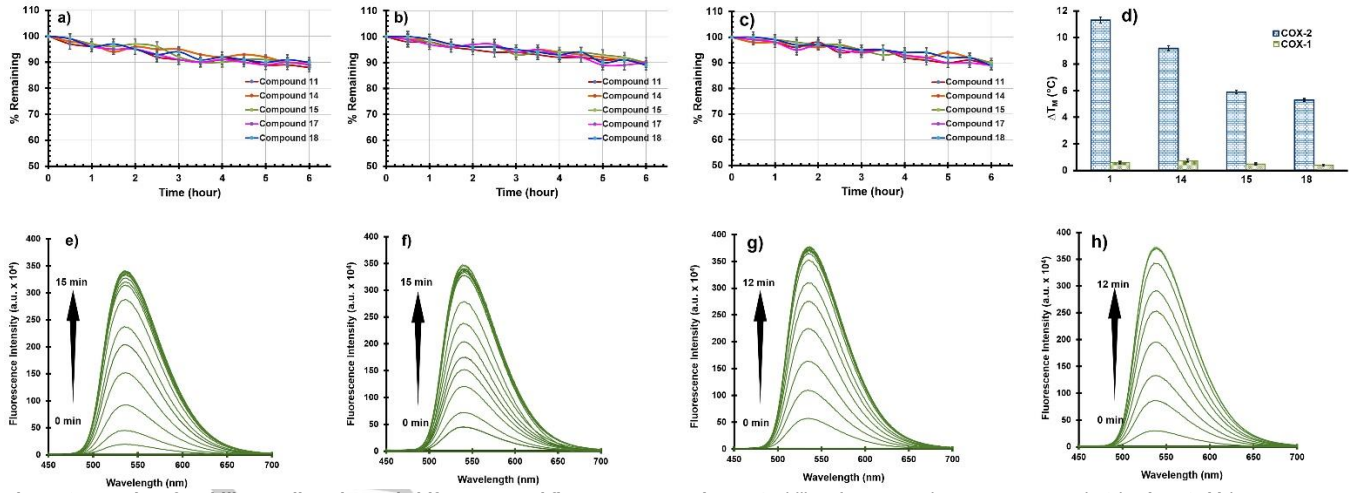

Figure 2. ***Results of stability studies, thermal shift assay, and fluorescence analyses.*** Stability of compound **11**, **14**, **15**, **17** and **18** in **a)** PBS, **b)** human serum **c)** rat serum, (n = 3, ± SEM); **d)** thermal melting temperature shifts of compound **1, 14, 15** and **18** upon binding to COX-1 and COX-2, the results are reported as the difference in melting temperature (ΔT_M) between ligand-bound and apo state of COX-2 (blue) and COX-1 (green). Melting temperature measurements made in triplicate ± SEM. **e)** Change in fluorescence emission over the time, upon the incubation of celecoxib-azide **14** (2 μL, 1 mM, 1% DMSO PBS,) with $CuSO_4$ (1 μL, 50 mM), sodium ascorbate (50 μL, 100 mM) and TBTA (2 μL, 50 mM) and **11** (1 μL, 100 mM) in the presence of either human recombinant COX-2 (95 μL) or **f)** HCA-7 lysate (protein concentration 1 mg mL^{-1}) at 37 °C. **g)** Change in fluorescence emission over the time, upon the incubation of **14** (2 μL, 1 mM, 1% DMSO in PBS) with **17** (1 μL, 100 mM) in presence of human recombinant COX-2 protein, **h)** HCA-7 lysate (protein concentration 1 mg mL^{-1}) at 37 °C. The change in fluorescence intensity was recorded at λ_{ex} = 490 nm, and for e) λ_{em} = 537 nm, f) λ_{em} = 541 nm, g) λ_{em} = 538 nm, h) λ_{em} = 539 nm. Data expressed as the mean of three measurements.

10.1002/chem.202003315

Binding of compound **15** (ΔT_M = 5.9 °C) and **18** (ΔT_M = 5.3 °C) also resulted in a stabilization in the COX-2 protein. However, no significant shift in melting temperature was measured upon incubating compounds **14**, **15,** and **18** (ΔT_M = <1 °C) with COX-1, which also confirmed their weak COX-1 inhibitory potency.

Next, we performed model reactions between celecoxib-azide **14** and NBD-alkyne **11** or NBD-DBCO **17** in the presence of human recombinant COX-2 protein or HCA-7 cell lysate to measure real-time fluorescence changes and viability of the click chemistry reaction in a proteinaceous environment (Figure 2e to 2h). Native fluorescence of celecoxib-azide **14** was undetectable after incubation with COX-2 protein or cell lysate
Time-dependent changes in fluorescence emission were recorded for Cu(I)-mediated click chemistry reaction of celecoxib-azide **14** and NBD-alkyne **11** in the presence of either human recombinant COX-2 protein or HCA-7 cell lysate (Figures 2e and 2f). Enhancement in fluorescence intensity was noticed immediately, and signal saturation was reached within 15 min, representing the completion of the click chemistry reaction and formation of fluorescent compound **15** (Figures 2e and 2f). The sole formation of 1,4-triazole **15** as the desired regioisomer was confirmed by LC/MS analyses and comparison with the HPLC profiles with the respective reference compound. Similarly, a noticeable enhancement in fluorescence intensity was observed during Cu-free click chemistry reaction between celecoxib-azide **14** and NBD-DBCO **17** to form compound **18** in the presence of pure COX-2 protein or cell lysate (Figure 2g and 2h). From these experiments, we concluded that all three compounds (**11**, **14**, and **17**) are suitable candidates for click chemistry reactions in a proteinaceous environment, and their corresponding fluorescent products **15** and **18** are formed within short reaction time.

In cellulo generation of fluorescent imaging probes 15 and 18 in COX-2-expressing colorectal cancer cells.
Based on collected COX-2 inhibitory activity profiles, fluorescence emission data, and COX-2 active site binding properties, celecoxib-azide **14** was selected as COX-2 binding compound in living cells. Compound **11** and **17** possessing clickable functionality were selected as complementary compounds. Presence and perinuclear expression of COX-2 in human colorectal cancer HCA-7 cells was confirmed with immunostaining experiments using anti-COX-2 monoclonal antibody. Cell culture was supplemented with non-fluorescent COX-2 binding compound celecoxib-azide **14** and incubated for 15 min. Cells were washed to remove unbound material and used in fluorescence imaging (Figure 3a, t = 0 min). Then, cells were treated with NBD-alkyne **11** in the presence of biocompatible and BTTPS/Cu^{I} click chemistry reagent solution [50 μM $CuSO_4$, 300 μM BTTPS (a water-soluble analog of TBTA), 2.5 mM sodium ascorbate in PBS].[60] The cells were imaged in 30 s time intervals, and after 5 min the perinuclear region of colorectal cancer cells began to fluoresce. Maximum fluorescence intensity was detected after 15 min (Figure 3b and 3c, t = 15 min after treating cells with **11**) demonstrating successful *in cellulo* click chemistry generation of the fluorescent imaging probe **15**.
After conducting a series of experiments by varying the incubation time (1 to 30 min) and amount of both click chemistry building blocks **11** and **14** (0.1 to 100 μM), we concluded that optimized conditions for successful imaging of COX-2 in HCA-7 through the formation of fluorescent compound **15** required a total 20 min incubation time [first compound **14** (1 μM, 5 min incubation), followed by compound **11** (1 μM, 15 min incubation)].
In contrast, extended incubation time (more than 80 min) and higher amount (150 μM) was needed for the visualization of COX-2 in HCA-7 cells when fluorescent celecoxib-T-NBD **15** was used directly (Figure 3e and 3f). The shorter incubation time (20 min *versus* 80 min) and the smaller amount of starting materials (1 μM for compounds **11** and **14** *versus* 150 μM for compound **15**) demonstrate the advantage of *in cellulo* assembly of imaging probe **15** over the use of pre-synthesized compound **15**.

Cells remained non-fluorescent in control experiments, where HCA-7 cells were incubated only with compounds **11** or **14** or BTTPS/Cu^{I} catalyst or PBS. We also performed blocking experiments to confirm COX-2 specificity of *in cellulo* generation of fluorescent celecoxib-T-NBD **15**. For this purpose, HCA-7 cells were pre-incubated with COX-2 inhibitor celecoxib (**1**, 1-100 μM) for 15 min, and the same experimental conditions (sequential addition of celecoxib-azide **14**, NBD-alkyne **11**, and BTTPS/Cu^{I} catalyst) were applied, and no fluorescence signal was detected (Figure 3d). The lack of a fluorescent signal in the HCA-7 cells during the blocking experiments confirmed the accessibility of the COX-2 active site for accommodating COX-2 binding compound **14** as a crucial step within the *in cellulo* formation process of fluorescence imaging probe **15**.
Non-specific binding and COX-2 selectivity during *in cellulo* click chemistry were further studied with the use of COX-2 negative HCT-116 cells. No significant fluorescence signal was detected upon the stepwise addition of click chemistry reagents, [celecoxib-azide **14** (1 μM), NBD-alkyne **11** (1 μM), and BTTPS/Cu^{I} catalyst reagent solution (50 μM $CuSO_4$, 300 μM BTTPS, 2.5 mM sodium ascorbate in PBS)] in HCT-116 cells (Figure S6).

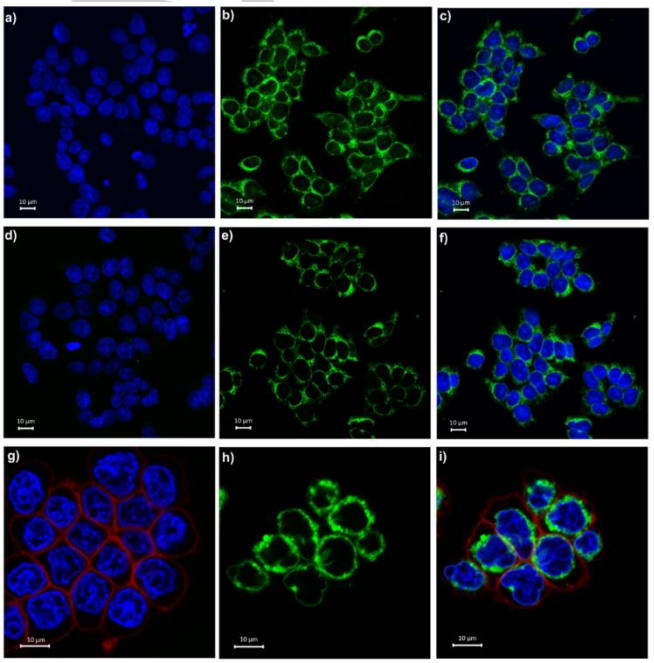

Figure 3. *In cellulo* click fluorescence imaging of COX-2 upregulation in colorectal cancer cells (HCA-7). a) HCA-7 cells treated with COX-2 binding compound celecoxib-azide **14**; b) COX-2 labeling in perinuclear region by incubating HCA-7 cells with celecoxib-azide **14**, pro-fluorophore **11**, and BTTPS/Cu^{I} for 15 min (nuclear staining not shown); c) Merged image of both nuclei and perinuclear staining (green) as a result of *in cellulo* click chemistry generation of fluorescence imaging probe celecoxib-T-NBD **15**; d) Cells pre-treated with COX-2 inhibitor celecoxib (**1**, 1 μM) prior to click chemistry (merged image); e) Cells treated with pre-synthesized celecoxib-T-NBD **15** (nuclear staining not shown); f) Merged image after incubation of pre-synthesized celecoxib-T-NBD **15**; g) live HCA-7 cells treated with celecoxib-azide **14**; h) live HCA-7 cells after *in cellulo* click chemistry generation of compound **15** (nuclear and plasma membrane staining not shown); i) tri-color live cell imaging using plasma membrane dye (red), nuclear stain(blue) and *in cellulo* generated fluorescent probe **15** (green). Nuclei were stained with 4′,6-diamidino-2-phenylindole (DAPI) in a) to f), and Hoechst dye was used in images g) to i).

In addition to the above-described control and blocking experiments, this experiment further confirmed the high COX-2 specificity of celecoxib-azide **14** and the involvement of COX-2 enzyme for the *in cellulo* generation of fluorescent imaging probe **15**. As COX-2 is mainly expressed in the perinuclear region (endoplasmic reticulum), we also used a cytoplasmic membrane dye (red) to differentiate the distinct perinuclear green labeling

10.1002/chem.202003315

from the red-colored cytoplasmic membrane and to demonstrate the generation of fluorescent celecoxib-T-NBD **15** in the perinuclear region of colorectal cancer cells, (Figure 3h and 3i).
This methodology was further tested in a Cu-free environment using strain-promoted fluorogenic click chemistry between celecoxib-azide **14** and NBD-DBCO **17**. Live HCA-7 cells were imaged in a temperature-controlled (37 °C) and humidified imaging chamber installed on a confocal microscope. Within 2 min, the perinuclear region of the cells triggered to green fluorescence, and fluorescence intensity increased over time, reaching the most intense fluorescence signal after 7 min (Figure 4a-4d and Figure 5).
The observed perinuclear fluorescence-labeling pattern was similar to that of the Cu (I)-catalyzed click chemistry reaction. However, strain-promoted *in cellulo* generation of fluorescence probe **18** and respective labeling of COX-2 was faster compared to the BTTPS/Cu^{I}-catalyzed click chemistry generation of compound **15**. Pre-treatment of HCA-7 cells with selective COX-2 inhibitor celecoxib **1** before the addition of complementary click chemistry building blocks **14** and **17** resulted in no fluorescence signal (Figure 4e). Likewise, no fluorescence signal was detected in COX-2 negative HCT116 cells confirming the COX-2 specificity of the reaction. In contrast to fluorescence labeling of COX-2 in HCA-7 cells using celecoxib-NBD (**15**, Figure 5e and 5f), no significant fluorescent signal was detected with compound **18** at concentrations ranging from 1 μM to 200 μM (Figure S11). This observation points to some central limitations such as reduced cell permeability of pre-synthesized and rather large fluorescent imaging probes like compound **18** for the detection of intracellular targets. However, when compound **18** was assembled within the cells by a fluorogenic click chemistry between complementary celecoxib-azide **14** and NBD-DBCO **17**, compound **18** produced a strong fluorescence signal (Figure 6b-6d). We also performed *in cellulo* click chemistry with compounds **14** and **17** in the presence of cell membrane dye (red) to confirm the generation of fluorescent probe **18** in the perinuclear region. Tri- color imaging in live HCA-7 cells provided superb details and confirmation that the *in cellulo* fluorogenic click chemistry occurred exclusively in the perinuclear region (Figure 4c and Figure 4d).

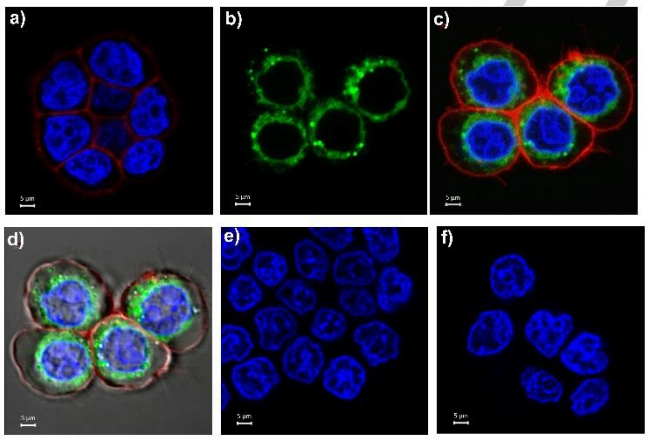

Figure 4. *In cellulo* fluorogenic click chemistry imaging of COX-2 in living cells (HCA-7). a) Live HCA-7 cells incubated with celecoxib-azide **14**; b) Visualization of COX-2 after *in cellulo* generation of imaging probe **18** starting from compounds **14** and **17** (nuclear staining not shown); c) Tri-color live cell imaging using plasma membrane dye (red), nuclear stain (blue) and *in cellulo* generated fluorescent probe **18** (green); d) Tri-color bright field imaging, highlighting the perinuclear *in cellulo* formation of fluorescent probe **18**; e) Cells pre-treated with celecoxib **1** before the fluorogenic click chemistry reaction between compounds **14** and **17**; f) Cells only treated with NBD-DBCO **17**. Hoechst dye used for nuclear staining.

We also performed a real-time live-cell imaging experiment to visualize the *in cellulo* generation of fluorescent probe **18** starting from compounds **14** and **17**, without washing HCA-7 cells.

Cells were cultured in sterile glass-bottom culture dishes suitable for live-cell microscopy. Throughout the experiment, optimal conditions (temperature: 37 °C, atmosphere: 5% CO_2 humidified environment) were maintained for cell survival, and the imaging data were collected in a single focal plane over time. Once in focus, the nuclear dye stained live HCA-7 cells were treated first with celecoxib-azide **14** (1 μM, 15 min incubation). Then, NBD-DBCO (**17,** 5 μM) was supplied and imaged continuously. Interestingly, no washing was necessary to record an evolving green fluorescence signal due to the *in cellulo* generation of fluorescent probe **18**. Cu-free *in cellulo* generation of fluorescent probe **18** in living cells occurred very rapidly and the perinuclear region of HCA-7 cells became distinctly fluorescent within 7 min as demonstrated by the recorded movie (see supplementary information) and the time-lapse images (Figure 5). No cell toxicity was noticed in a MTS assay, and HCA-7 cells remained healthy while undergoing cell division over several hours (Figure S10). To our best knowledge, this experiment is the first report of a fast *in cellulo* fluorogenic click chemistry for the generation of a fluorescent imaging probe to study inflammation and cancer biomarker COX-2 in living cells over time.

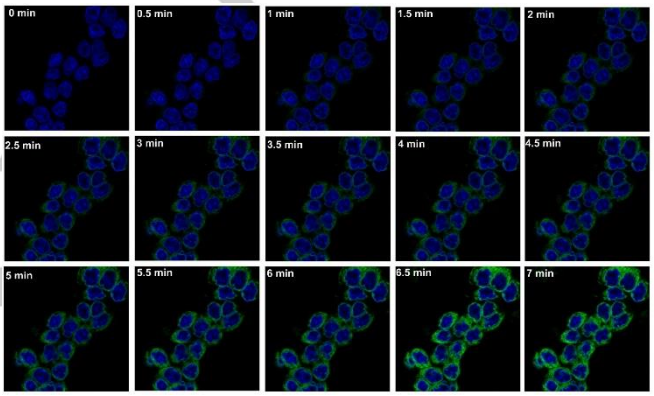

Figure 5. Time-lapse fluorescence images demonstrating the *in cellulo* formation of fluorescent probe 18 in living cells. Time series montage showing the generation of fluorescence probe **18** upon fluorogenic click chemistry reaction between celecoxib-azide **14** and NBD-DBCO **17** in COX-2 expressing HCA-7 cells. Hoechst dye used for nuclear staining.

Computational analyses

We also carried out comprehensive molecular docking and MD simulation studies to investigate the binding mode of celecoxib-azide **14** (Figure 6 and Figure S7) and click chemistry products **15** and **18** (Figures S7 and S8) in the COX-2 active site. The top-ranked binding position suggested that celecoxib-azide **14** orientates favorably into the active site ($E_{intermolecular}$ = −13.9 kcal mol^{-1}) and exerts significant electrostatic interactions with residues of the COX-2 active site (Figure 6, Figures S3 and S4). One of the *O*-atom of *para*-sulfonamide H-bonded with H90 (distance O---N = 2.54 Å) present in the secondary pocket and the *N*-atom of *para*-sulfonamide showed H-bonding with S353 (N---O = 2.71 Å). The 4-CH_3-phenyl was oriented towards the entrance of the hydrophobic pocket lined by Y385, M522, W387, L384, F518 residues, whereas the CF_3-group present on pyrazole ring was located in a small cavity lined by V349, L359, and V116. Another interesting information from the molecular docking studies revealed the peculiar orientation of the azide group (-N_3) in compound **14**. It appeared that the azide group was dangled out from a hole like arrangement of amino acid residues (Figure 6), demonstrating favorable accessibility of the azide group for click chemistry reactions with complementary molecules. Protein-ligand (PL) interaction analyses showed that the pyrazole ring was located in the vicinity of R120 (distance between the center of mass of the ring and the guanidine moiety = 5.15 Å) and showed cation–π and π-π interactions with R120 (Figure S4).

10.1002/chem.202003315

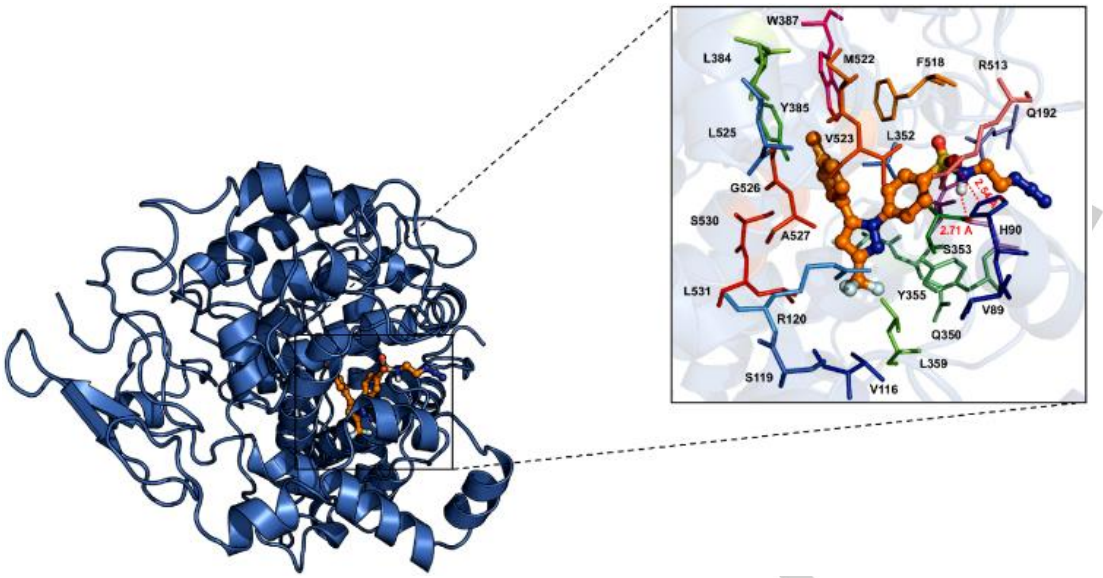

Figure 6. Computational analysis for the binding of celecoxib-azide 14 to COX-2. Molecular docking experiments of celecoxib-azide **14** to COX-2 (PDB ID: 6COX). Important amino acid residues are shown and H-bonding interactions are displayed in red color.

We also performed 100 ns MD simulations for the celecoxib-azide **14**-COX-2 complex (COX-2_{14}) to investigate the binding of celecoxib-azide **14** with COX-2 in dynamic settings. We found that celecoxib-azide **14** preserved its binding mode and critical interactions with active site residues in a dynamic environment (Figure S9). Time evolution of the root means square deviation (RMSD) analyses using a 100 ns trajectory revealed an early increase due to the equilibration of the system, followed by a stabilization conformation for the COX-2_{14} complex, and maintenance of an average RMSD 1.52 Å (Figure S9). Except for a few fluctuations between 12.1-16.5 ns (maximum RMSD = 1.71 Å), the trajectory remained stable over the time course of the simulation.

Conclusion

We have developed highly potent and COX-2 selective compound celecoxib-azide **14** capable of undergoing *in cellulo* fluorogenic click chemistry and the visualization of cytoplasmic COX-2 in living cells. Using comprehensive computational, pharmacological, and biophysical analyses, we validated that celecoxib-azide **14** is a suitable building block for *in cellulo* generation of a COX-2-specific fluorescent imaging probe. We demonstrated the use of cell-permeable COX-2 binding celecoxib-azide **14** and compound NBD-DBCO **17** for dynamic and real-time fluorescence imaging of COX-2 in living cells. The ability of celecoxib-azide **14** to bind selectively to COX-2 and trigger rapid fluorescence "turn on" signal upon *in cellulo* click chemistry represents a new chemical toolbox for the detection of intracellular biomarkers like COX-2 in living cells with high sensitivity. The basic principle and the modular nature of the novel chemical toolbox should also aid the development of other fluorescence imaging assays for targeting other intracellular disease biomarkers such as kinases and proteases in living cells.

Experimental Section

Material and Methods. Melting points were determined with a Thomas–Hoover capillary apparatus and are uncorrected. Proton nuclear magnetic resonance (^{1}H NMR, 600 MHz), carbon-13 nuclear magnetic resonance ^{13}C NMR (150 MHz), and fluorine-19 nuclear magnetic resonance (^{19}F NMR, 565 MHz) spectra were recorded on a Bruker AM-600 NMR spectrometer using $CDCl_3$ or DMSO-d_6 or CD_3OD as the solvent. Chemical shifts are reported in parts per million (ppm) with tetramethylsilane (TMS) as an internal reference, and *J* (coupling constant) values were estimated in Hertz (*Hz*). The following notation is used: br – broad, s – singlet, d – doublet, t – triplet, q – quartet, quin – quintet, m – multiplet, dd – doublet of doublets, ddd – doublet of doublets of doublets, dt – doublet of triplets, td – triplet of doublets. Mass spectra (MS) were recorded on a Water's Micromass ZQ 4000 mass spectrometer using the ESI ionization mode. The purity of the compounds was established by elemental analyses, which were performed for C, H, and N by the Microanalytical Service Laboratory, Department of Chemistry, University of Alberta, Canada. All synthesized compounds showed a single spot on Macherey–Nagel Polygram Sil G/UV254 silica gel plates (0.2 mm) using a low, medium, and highly polar solvent system, and no residue remained after combustion, indicating a purity >98%. Column chromatography was performed on a Combiflash Rf system using gold-silica columns, size ranging from small, medium, and large. All reagents purchased from the Aldrich Chemical Co. (Milwaukee, WI, USA) were used without further purification. DMSO, ethanol as well as PBS buffer, prepared with Millipore-filtered water (resistivity >18 MΩcm^{-1} at 20 °C), were from Sigma-Aldrich (molecular biology grade). All reactions monitored by thin-layer chromatography (TLC) on silica gel plates (60 F254; Merck) visualizing with I_2 and ultraviolet light (UV). Compounds **4, 6,** and **11** were synthesized by using previously reported procedures,[61-63], and the synthetic routes are described in Supplementary Scheme S1-S3. Quantum yields were calculated by methods described by Crosby and Demas[64] using fluorescein and quinine sulfate as standards. Stock solutions in DMSO were diluted into water or PBS in a 1cm x 1cm quartz cuvette and the slit width was 4 nm. All the measurements were made in at least triplicate. All analytical LC/MS analyses were performed on a Water's Micromass ZQTM 4000 LC-MS instrument.

Synthesis of *N*-((1-(7-(diethylamino)-2-oxo-2H-chromen-3-yl)-1H-1,2,3-triazol-4-yl)methyl)-4-(5-(*p*-tolyl)-3-(trifluoromethyl)-1H-pyrazol-1-yl)benzenesulfonamide 5: 3-Azido-7-(diethylamino)-2H-chromen-2-one **4** (154 mg, 0.6 mmol) and *N*-(prop-2-yn-1-yl)-4-(5-(p-tolyl)-3-(trifluoromethyl)-1H-pyrazol-1-yl)benzenesulfonamide **3** (251 mg, 0.6 mmol) were stirred together in ethanol and water (v/v = 2:1, 5 mL). To this reaction mixture was

added copper (II) sulfate dissolved in water (0.5 M, 1 mol %) and aqueous sodium ascorbate (0.1 M, 10 mol %). The reaction mixture was stirred at room temperature and reaction progress was monitored by TLC. Upon completion (1 h), the ethanol was removed under reduced pressure and the residue was dissolved ethyl acetate (20 mL) and washed H_2O (5 mL), with brine (5 mL). The organic fraction was separated, dried over anhydrous $MgSO_4$ and evaporated under reduced pressure. The crude product was purified by flash column chromatography using a mixture of 2-5 % MeOH in CH_2Cl_2 as eluent to furnish pure title compound **5** as white solid in 82.5 % yield. ^{1}H-NMR (DMSO-d_6, 600 MHz) δ 1.13 (t, J = 7.2 Hz, 6 H, 2 x CH_3), 2.30 (s, 3 H, CH_3), 3.48 (q, J = 7.2 Hz, 4 H, 2 x CH_2), 4.20 (s, 2 H, CH_2), 6.64 (d, J = 1.8 Hz, 1 H, Ar-H), 6.82 (dd, J = 9.0 Hz, J = 1.8 Hz, 1 H, coumarin-ring- *H*), 7.18 (s, 1 H, C*H* of pyrazole ring), 7.19 (d, J = 8.4 Hz, 2 H, Ar-H), 7.21 (d, J = 8.4 Hz, 2 H, Ar-H), 7.52 (d, J = 8.4 Hz, 2 H, Ar-H), 7.41 (d, J = 9.0 Hz, 1 H, coumarin-ring- *H*), 7.83 (d, J = 8.4 Hz, 2 H, Ar-H), 8.32 (s, 1 H, coumarin-ring- *H*), 8.38 (s, 1 H), 8.43 (broad s, 1 H, N*H*); ^{13}C NMR (DMSO-d_6, 150 MHz): δ 12.76 (2 x *C*H$_3$), 21.38 (*C*H$_3$), 38.39 (*C*H$_2$), 44.69 (2 x *C*H$_2$), 96.84 (coumarin-ring), 106.64 (*C*H of pyrazole ring), 106.91 (coumarin-ring-Ar-*C*H), 110.10 (coumarin-ring-Ar-*C*H), 118.19, 121.11 (q, $^1J_{C\text{-}F}$ = 267 Hz, *C*F$_3$), 124.59 (coumarin-ring-Ar-*C*H), 125.4 (*C*), 125.59 (Ar-*C*H), 126.50 (*C*), 128.21 (Ar-*C*H), 129.14 (Ar-*C*H), 129.91 (Ar-*C*H), 130.94 (coumarin-ring-Ar-*C*H), 130.12 (*C*), 137.00, 139.56, 141.99, 143.82 (q, ^2J = 36 Hz, pyrazole *C*3), 145.70, 151.91, 156.08, 157.09; ^{19}F (DMSO-d_6, 565 MHz): -60.90 (CF_3); EI-MS: 678.7 [M+H]$^+$; Anal. Calculated for $C_{33}H_{30}F_3N_7O_4S$: C, 58.49; H, 4.46; N, 14.47; S, 4.73; found: C, 58.42; H, 4.48; N, 14.49; S, 4.68.

Synthesis of N-((1-(7-nitrobenzo[c][1,2,5]oxadiazol-4-yl)-1H-1,2,3-triazol-4-yl)methyl)-4-(5-(*p*-tolyl)-3-(trifluoromethyl)-1H-pyrazol-1-yl)benzenesulfonamide 7: 4-Azido-7-nitrobenzo-[c][1,2,5]oxadiazole (**6**, 124 mg, 0.6 mmol) and *N*-(prop-2-yn-1-yl)-4-(5-(p-tolyl)-3-(trifluoromethyl)-1H-pyrazol-1-yl)benzene-sulfonamide **3** (251 mg, 0.6 mmol) were stirred together in ethanol and water (v/v = 2:1, 5 mL). To this reaction mixture was added copper(II)sulfate dissolved in water (0.5 M, 1 mol %) and aqueous sodium ascorbate (0.1 M, 10 mol %). The reaction mixture was stirred at room temperature and reaction progress was monitored by TLC. Upon completion (1 h), the ethanol was removed under reduced pressure and the residue was dissolved ethyl acetate (20 mL) and washed H_2O (5 mL), with brine (5 mL). The organic fraction was separated, dried over anhydrous $MgSO_4$ and evaporated under reduced pressure. The crude product was purified by flash column chromatography using a mixture of 2-5 % MeOH in CH_2Cl_2 as eluent to furnish pure title compound **7** in 84.5 yield. ^{1}H-NMR ($CDCl_3$, 600 MHz) δ 2.36 (s, 3 H, CH_3), 4.47 (s, 2 H, CH_2), 6.84 (s, 1 H, C*H* of pyrazole ring), 7.14 (d, J = 8.4 Hz, 2 H, Ar-H), 7.21(d, J = 8.4 Hz, 2 H, Ar-H), 7.36 (d, J = 8.4 Hz, 2 H, Ar-H), 7.83 (d, J = 8.4 Hz, 2 H, Ar-H), 8.38 (d, J= 7.8 Hz, 1 H, Ar-H), 8.72 (s, 1 H), 8.76 (d, J = 7.8, 1 H, Ar-H); ^{13}C NMR ($CDCl_3$, 150 MHz): 21.17 (*C*H$_3$), 41.71 (*C*H$_2$), 106.35 (*C*H of pyrazole ring), 117.45, 119.48, 120. 52, 121.13 (q, $^1J_{C\text{-}F}$ = 267 Hz, *C*F$_3$), 125.4 (Ar-*C*H), 125.7 (4-methylphenyl *C*1), 128. 4 (Ar-*C*H), 128.7 (Ar-*C*H), 129.7 (Ar-*C*H), 131.81, 132.45, 135.4, 139.2, 139.8, 142.6, 143.11, 143.4 (q, ^2J = 36 Hz, pyrazole *C*3), 145.2, 149.54; ^{19}F ($CDCl_3$, 565 MHz,): -62.19 (CF_3); EI-MS: 626.5 [M+H]$^+$; Anal. Calculated for $C_{26}H_{18}F_3N_9O_5S$: C, 49.92; H, 2.90; N, 20.15; S, 5.13, found: C, 49.90; H, 2.96; N, 20.11; S, 5.09.

Synthesis of *N*-(3-(4-(((7-nitrobenzo[c][1,2,5]oxadiazol-4-yl)-amino)methyl)-1H-1,2,3-triazol-1-yl)propyl)-4-(5-(p-tolyl)-3-(trifluoromethyl)-1H-pyrazol-1-yl)benzenesulfonamide 12: *N*-(3-Azidopropyl)-4-(5-(*p*-tolyl)-3-(trifluoromethyl)-1H-pyrazol-1-yl)-benzenesulfonamide **9** (200 mg, 0.44 mmol) and 7-nitro-N-(prop-2-yn-1-yl)benzo[c][1,2,5]oxadiazol-4-amine **11** (0.44 mmol) and were stirred together in ethanol and water (v/v = 2:1, 5 mL). To this reaction mixture was added copper (II) sulfate dissolved in water (0.5 M, 1 mol %) and aqueous sodium ascorbate (0.1 M, 10 mol %). The reaction mixture was stirred at room temperature and reaction progress was monitored by TLC. Upon completion (1 h), the ethanol was removed under reduced pressure and the residue was dissolved ethyl acetate (20 mL) and washed H_2O (5 mL), with brine (5 mL). The organic fraction was separated, dried over anhydrous $MgSO_4$ and evaporated under reduced pressure. The crude product was purified by flash column chromatography using a mixture of 2-5 % MeOH in CH_2Cl_2 as eluent to furnish pure title compound **12** in 85 % yield as a white solid. ^{1}H-NMR (CD_3OD, 600 MHz) δ 2.23 (s, 3 H, CH_3), 2.80-2.91 (m, 2H, CH_2), 3.24-3.28 (m, 2 H, CH_2), 4.32-4.37 (m, 2 H, CH_2), 4.36 (s, 2 H, CH_2), 6.38 (d, J = 9.0 Hz, 1 H, NBD-ring), 6.86 (s, 1 H, C*H* of pyrazole ring), 7.02-7.07 (m, 4H, Ar-H), 7.35-7.41 (m, 2 H, Ar-H), 7.65-7.72 (m, 2 H, Ar-H), 7.85 (s, 1 H), 8.34 (d, J = 9.0 Hz, NBD-ring); ^{13}C NMR (CD_3OD, 150 MHz):19.86 (CH_3), 29.41 (*C*H$_2$), 39.26 (*C*H$_2$), 43.31 (*C*H$_2$), 51.21 (*C*H$_2$), 105.51 (*C*H of pyrazole ring), 121.04 (q, $^1J_{C\text{-}F}$ = 267 Hz, *C*F$_3$), 122.30 (*C*-NO$_2$), 123.82 (NBD-ring *C*H), 125.69 (*C*), 125.88 (Ar-*C*H), 127.51 (Ar-*C*H), 128.69 (Ar-*C*H), 129.29 (Ar-*C*H), 131.41, 132.38 (*C*), 134.48 (*C*), 136.89 (NBD-ring *C*H), 139.66 (*C*), 140.39, 142.39, 143.69, 144.07 (q, ^2J = 36 Hz, pyrazole *C*3),144.65, 145.78; ^{19}F (CD_3OD, 565 MHz): -63.91 (CF_3); EI-MS: 683.1 [M+H]$^+$; Anal. Calculated for $C_{29}H_{25}F_3N_{10}O_5S$: C, 51.03; H, 3.69; N, 20.52; S, 4.70; found: C, 51.08; H, 3.62; N, 20.59; S, 4.78.

Synthesis of *N*-(2-(4-(((7-nitrobenzo[c][1,2,5]oxadiazol-4-yl)-amino)methyl)-2H-1,2,3-triazol-2-yl)ethyl)-4-(5-(p-tolyl)-3-(tri-fluoromethyl)-1H-pyrazol-1-yl)benzenesulfonamide 15: N-(2-Azidoethyl)-4-(5-(*p*-tolyl)-3-(trifluoromethyl)-1H-pyrazol-1-yl)-benzenesulfonamide **14** (200 mg, 0.44 mmol) and 7-nitro-N-(prop-2-yn-1-yl)benzo[c][1,2,5]oxadiazol-4-amine **11** (96 mg 0.44 mmol) and were stirred together in ethanol and water (v/v = 2:1, 5 mL). To this reaction mixture was added copper (II) sulfate dissolved in water (0.5 M, 1 mol %) and aqueous sodium ascorbate (0.1 M, 10 mol %). The reaction mixture was stirred at room temperature and reaction progress was monitored (TLC). Upon completion (1 h), the ethanol was removed under reduced pressure and the residue was dissolved ethyl acetate (20 mL) and washed H_2O (5 mL), with brine (5 mL). The organic fraction was separated, dried over anhydrous $MgSO_4$ and evaporated under reduced pressure. The crude product was purified by flash column chromatography using a mixture of 2-5 % MeOH in CH_2Cl_2 as eluent to furnish pure title compound **15** in 88.5 % yield as a white solid. ^{1}H-NMR (CD_3OD, 600 MHz) δ 2.23 (s, 3 H, CH_3), 3.27-3.29 (m, 2 H, HN-CH_2-CH$_2$), 4.36-4.38 (m, 2 H, HN-CH$_2$-CH_2), 4.39 (s, 2 H, CH_2), 6.33 (d, J = 9.0 Hz, 1 H, NBD-ring), 6.81 (s, 1 H, C*H* of pyrazole ring), 7.04-7.09 (m, 4H, Ar-H), 7.38-7.40 (m, 2 H, Ar-H), 7.69-7.71 (m, 2 H, Ar-H), 7.86 (s, 1 H), 8.39 (d, J = 9.0 Hz, NBD-ring); ^{13}C NMR (CD_3OD, 150 MHz):19.86 (CH_3), 37.23 (*C*H$_2$), 42.35 (*C*H$_2$), 52.23 (*C*H$_2$), 105.58 (*C*H of pyrazole ring), 121.06 (q, $^1J_{C\text{-}F}$ = 267 Hz, *C*F$_3$), 122.34 (*C*-NO$_2$), 123.88 (NBD-ring *C*H), 125.68 (*C*), 125.81 (Ar-*C*H), 127.59 (Ar-*C*H), 128.64 (Ar-*C*H), 129.23 (Ar-*C*H), 131.43, 132.31 (*C*), 134.43 (*C*), 136.81 (NBD-ring *C*H), 139.66 (*C*), 140.31, 142.33, 143.63, 144.01 (q, ^2J = 36 Hz, pyrazole *C*3),144.60, 145.73; ^{19}F (CD_3OD, 565 MHz): -63.91 (CF_3); EI-MS: 669.6 [M+H]$^+$; Anal. Calculated for $C_{28}H_{23}F_3N_{10}O_5S$: C, 50.30; H, 3.47; N, 20.95; S, 4.80; found: C, 50.28; H, 3.42; N, 20.91; S, 4.84.

Synthesis of NBD-DBCO 17: Into a solution of 4-chloro-7-nitrobenzo[c][1,2,5]oxadiazole **10** (200 mg, 1 mmol) in 10 mL dry THF, DBCO-amine **16** (276 mg, 1 mmol) and dry triethylamine (1 mmol) were added. The reaction mixture was stirred at 25 °C, and the progress was monitored by TLC, upon completion (1 h), the solvent was evaporated in reduced pressure, and the residue was dissolved CH_2Cl_2 and the organic fraction was washed with brine and then dried over anhydrous Na_2SO_4 and evaporated under reduced pressure. The crude product was purified by flash column chromatography using a mixture of 2-5 % MeOH in CH_2Cl_2 as eluent to furnish pure compound **17** in 88% yield as a thick liquid. ^{1}H NMR ($CDCl_3$, 600 MHz): δ 2.28 (ddd, J = 15.6 Hz, J = 8.1 Hz, J = 4.2 Hz, 1 H of CH_2), 2.54 (ddd, J = 15.6 Hz, J = 8.1 Hz, J = 4.2 Hz, 1 H of CH_2), 3.41-3.45 (m, 2 H, CH_2), 3.61 (d, J = 13.8 Hz, 1 H of CH_2), 5.08 (d, J = 13.8 Hz, 1 H of CH_2), 5.84

(d, *J* = 8.4 Hz, 1 H , NBD ring), 6.54 (broad s, 1 H, N*H*), 6.94 (d, *J* = 8.4 Hz, 1 H, DBCO ring), 7.16-7.36 (m, 6 H), 7.58 (d, *J* = 7.8, 1 H, DBCO ring), 8.22 (d, *J* = 8.4 Hz, 1 H, NBD ring); ^{13}C NMR ($CDCl_3$, 150 MHz): 33.52 (-CO-CH_2), 39.93 (CH_2), 55.55 (CH_2), 98.37 (NBD ring *C*H), 107.11 (≡*C*), 115.10 (*C*≡), 122.50 (*C*), 122.71 (*C*), 123.85 (*C*),125.54 (*C*H), 127.40 (*C*H), 127.80 (*C*H), 128.43 (*C*H), 128.63 (*C*H), 128.74 (*C*H), 128.83 (CH), 132.16 (*C*H), 136.31 (*C*H), 143.48 (*C*), 143.83 (*C*), 144.15 (*C*), 144.42 (*C*), 150.78 (*C*), 170.64 (C=O); Φ_F = 0.51, 1% DMSO in PBS; EI-MS: 440.4 $[M+H]^+$; Anal. Calculated for $C_{24}H_{17}N_5O_4$: C, 65.60; H, 3.90; N, 15.94; found: C, 65.64; H, 3.86; N, 15.90.

Synthesis of *N*-(2-(8-(3-((7-nitrobenzo[c][1,2,5]oxadiazol-4-yl)amino)propanoyl)-8,9-dihydro-3H-dibenzo[b,f][1,2,3]triazolo[4,5-d]azocin-3-yl)ethyl)-4-(5-(p-tolyl)-3-(trifluoromethyl)-1H-pyrazol-1-yl)benzenesulfonamide 18: Into a solution of 4 *N*-(2-azidoethyl)-4-(5-(*p*-tolyl)-3-(trifluoromethyl)-1H-pyrazol-1-yl)-benzenesulfonamide **14** (50 mg, 0.11 mmol) in 10 mL of methanol, NBD-DBCO **17** (48 mg, 0.11 mmol) was added and the reaction mixture was stirred at 25 °C, and the progress was monitored by TLC, upon disappearance of stating material on TLC, the solvent was evaporated in reduced pressure, and crude product was purified by flash column chromatography using a mixture of 2-5 % MeOH in CH_2Cl_2 as eluent to furnish pure compound **18** in 85% yield as a yellow solid. ^{1}H-NMR ($CDCl_3$, 600 MHz) δ 2.10-2.13 (m, 2H, CH2), 2.29 (s, 3 H, CH3), 3.01-3.03 (m, 2H, CH2), 3.45-.3.49 (m, 2 H, CH2), 4.35-4.38 (m, 1H), 4.52-4.71 (m, 2H, CH2), 6.18 (s, 1 H NH), 6.23 (d, *J* = 8.4 Hz, 1 H, NBD ring), 6.30 (t, *J* = 9.5 Hz, 1 H), 6.55 (s, 1 H, pyrazole ring), 6.75 (broad s, 1 H, N*H*), 6.96 (dd, *J* = 7.4 Hz, *J* = 0.9 Hz, 1 H), 7.02 (d, *J* = 8.4 Hz, 2 H), 7.09 (d, *J* = 8.4 Hz, 2 H), 7.21-7.31 (m, 3 H), 7.35-7.37 (m, 2 H), 7.46 (m, 2 H), 7.66-7.68 (m, 1 H), 7.73-7.75 (m, 2 H), 8.36 (d, *J* = 8.4 Hz, 1 H, NBD ring);^{13}C NMR ($CDCl_3$, 150 MHz): δ 21.33 (CH_3), 33.00 (-CO-CH_2), 42.51 (CH_2), 50.45 (CH_2), 52.03 (CH_2), 61.64 (CH_2), 101.34 (NBD ring *C*H), 106.28 (*C*H of pyrazole ring), 121.98 (q, $^1J_{C\text{-}F}$ = 267 Hz, *C*F_3), 123.66 (C), 123.86 (C), 125.54 (Ar-*C*H), 125.61 (C),126.65, 127.78, 127.92, 128.70, 129.71, 129.77, 130.07, 130.12, 130.16, 130.82, 131.29, 131.47 (C), 134.54 (C), 136.56 (CH), 139.61 (C), 139.71 (C), 139.85 (C), 142.51 (C), 142.68 (C), 143.70 (C), 143.96 (C), 144.02 (q, ^2J = 36 Hz, pyrazole *C*3), 144.21 (C), 144.47 (C), 145.26 (C), 173.56 (C=O); Φ_F = 0.75, 1% DMSO in PBS; EI-MS: 890.3 $[M+H]^+$; Anal. Calculated for $C_{43}H_{34}F_3N_{11}O_6S$: C, 58.04; H, 3.85; N, 17.31; S, 3.60; found: C, 58.09; H, 3.81; N, 17.37; S, 3.57.

COX inhibition assay. The ability of known COX-2 selective inhibitor celecoxib **1**, celecoxib-alkyne **3**, celecoxib-azides **9** and **14**, and target compounds **5**, **7**, **12**, **15** and **18** to inhibit ovine COX-1 and recombinant human COX-2 was determined using a COX inhibitor assay (Cayman Chemical, Ann Arbor, USA; item number: 700100) following the manufacturer's protocol. Each compound assayed in a concentration range of 10^{-9} M to 10^{-3} M, in triplicate. PRISM5 software used to calculate IC_{50} values. In addition to celecoxib, both Dup-697 (potent COX-2 inhibitor) and SC-560 (potent COX-1 inhibitor) used as internal controls during screening all compounds.

Based on the in-vitro COX-2 inhibitory data, compounds **3, 5, 7, 9, 12, 14, 15, 18,** and celecoxib **1** were further evaluated of cellular COX-2 inhibitory activity in COX-2 overexpressing live HCA-7 cells (colorectal cancer cell line, COX-2 expression was confirmed with immunoblotting). The HCA-7 cells were cultured in T75 flasks using DMEM/F12 (1:1) medium supplemented with 10% (v/v) fetal bovine serum (GIBCO, 12483), 2 mM L-glutamine (GIBCO, 25030), 1% penicillin/streptomycin and 20 mM HEPES buffer (GIBCO, 15630) and were kept in a 37 ºC humidified incubator with the supply of 5% CO_2 in air. Cells washed three times for 5 min with 1 ml PBS. Cells negatively tested for mycoplasma contamination either by the vendor or in house. Cells incubated with test compounds, reference drug celecoxib (**1**), or vehicle (solvent) at a concentration range of 10^{-9} M to 10^{-3} M. After 30 min incubation, the reaction stopped on ice, supernatants taken, and COX-2 mediated production of PGE2 was immediately determined using prostaglandin E metabolite ELISA kit (514010, Cayman Chemical, Ann Arbor, MI, USA). The PGE2 concentration quantified by following manufacturer assay procedure. All experiments were performed three times, and ±S.E.M. values were calculated. The known selective COX-2 inhibitor celecoxib was used as a control, and for a competition experiment, cells were pre-treated with (1-100 μM) celecoxib before the treatment of test compounds. The PRISM5 software was used to calculate IC_{50} values.

Stability of compounds 11, 14, 15, 17, and 18 in PBS and in the presence of various additives. Stock solutions of compounds **11**, **14**, **15**, **17,** and **18** (10-50 mM range) were prepared in DMSO for molecular biology. A Solution of each compound (10-50 mM range) added into freshly thawed human serum (from human male AB plasma, USA origin, sterile-filtered, Sigma–Aldrich) at 37 °C; the final concentration of the test compound was 100 µM 500 µM. The resulting solution incubated at 37 °C and at various time intervals (0 to 30 h) 200 µL the reaction mixture samples taken and added to 200 µL of acetonitrile (biological grade) containing 0.1% trifluoroacetic acid to deproteinize the proteins. Into each sample mixture, 10 µL of an internal standard solution (2 mM solution in methanol) added. Sample mixture sonicated, vortexed, and then centrifuged for 15 minutes at 2150 x g, the clear supernatant transferred into the fresh tube for LC-MS analysis. Each sample was analyzed in triplicate by injecting (10 µl) into the LC/MS instrument with SIM mode, (Water's Micromass ZQTM 4000 LC−MS instrument, operating in the ESI-positive mode, equipped with a Water's 2795 separation module). For measuring a change in fluorescence intensity, 10 µL of a 10 mM stock of the test compound was transferred into PBS (1 mL) containing various additives or alternative solvent (1 mL), incubated at 37 °C and fluorescence was recorded each at a series of time points by following standard procedure.

Fluorescence studies. Tris[(1-benzyl-1H-1,2,3-triazol-4-yl)-methyl]amine (TBTA, 2 µL, 50 mM in PBS pH 7.4), $CuSO_4$ (1 µL, 50 mM in H_2O) were mixed with 944 µL PBS in a cuvette and sodium ascorbate (50 µL, 100 mM in PBS) added and the solution was mixed again. Then, human recombinant COX-2 protein (95 µL) and celecoxib-azide **14** [2 µL, 1 mM ethanol] were added and mixed gently. The native fluorescence emission of solution was measured (t = 0 s, λ_{ex} = 415 nm, λ_{em} = 420-800 nm). Then into this solution, either compound **11** (1 µL, 100 mM in ethanol) or **17** (1 µL, 100 mM in ethanol) were added, mixed and fluorescence emission measured after every 20 s until saturation of signal (λ_{ex} = 415 nm, λ_{em} = 420-800 nm). The native fluorescence intensity of **14** (1 µL, 100 mM) and **17** (1 µL, 100 mM) was found lower than respective triazole products **15** and **18** (λ_{ex} = 415 nm, λ_{em} = 420-800 nm). Quantum yield: Φ_F: fluorescence quantum yield.

Cell lysate. HCA-7 colony 29 cells (Sigma Aldrich, 02091238) with 80% confluence were used, the media was aspirated, the cells are kept on ice plate and washed twice with 10 mL ice-cold 1X PBS. The radio-immunoprecipitation assay (RIPA) buffer (400 µL) added to lyse the cells, incubated for 15 min, centrifuged at 13000 rpm for 5 min at 4 °C and the supernatant was collected. The protein concentration determined by the BCA assay (Thermo Scientific Pierce).

Computational analyses. Coordinates from the X-ray crystal structure of COX-1 (ovine, 1EQG, ibuprofen bound in the active site) and COX-2 (murine, 6COX, SC558 bound in the active site) were taken from the RCSB Protein Data Bank server. Compounds were constructed with the builder toolkit of the software package ArgusLab 4.0.1, and energy minimized using the semi-empirical quantum mechanical method PM3. The monomeric structure of the enzyme was selected, and the active site was defined as 15 Å

around the ligand. The molecule to be docked in the enzyme active site was inserted into the workspace carrying the structure of the enzyme. The docking program implements an efficient grid-based docking algorithm, which approximates an exhaustive search within the free volume of the binding site cavity. The conformational space was measured by the geometry optimization of the flexible ligand (rings are treated as rigid) in combination with the incremental construction of the ligand torsions. Thus, docking occurred between the flexible ligand parts of the compound and enzyme. The ligand orientation was determined by a shape scoring function based on A_{score} and the final positions were ranked by lowest interaction energy values. The $E_{interaction}$ value is the sum of the energies involved in hydrogen bond interactions, hydrophobic interactions, and van der Waals interactions. Each molecular docking experiment was repeated three times to confirm the reproducibility. Hydrogen bond and hydrophobic interactions between the compound and enzyme were explored by distance measurements. Molecular dynamics (MD) simulations were performed with AMBER18 (*University of California, San Francisco)*, the ff14SB force field was employed for the receptor, and the AMBER GAFF3 force field was used for ligands, and standard protocol described in the AMBER manual was followed (.[65,66] In brief, the initial coordinates for the protein atoms were taken from the X-ray structure of COX-2 (PDB ID code 6COX). The ligand was placed by the superposition of the best binding mode predicted from computational studies. Atom-centered partial charges were derived by using the AMBER antechamber program, after the geometry optimization at the B3LYP/6–31G* level. The octahedral box of TIP3P water molecules were extended (10 Å) from the protein, and the solvated system was neutralized with counterions (Na^+ and Cl^-) using LEaP. In the MD simulation protocol, the time step was chosen to be 2 fs, and the SHAKE algorithm was used to constrain all bonds involving hydrogen atoms. A nonbonded cutoff of 10.0 Å was used, and the nonbonded pair list was updated every 25-time steps. Langevin dynamics was used to control the temperature (300 K) using a collision frequency of 1.0/ps, with isotropic position scaling to maintain the pressure (1 atm). Periodic boundary conditions were applied to simulate a continuous system. To include the contributions of long-range interactions, the Particle-Mesh-Ewald (PME) method was used with a grid spacing of ~1 Å combined with a fourth-order B-spline interpolation to compute the potential and forces between grid points. The trajectories were analyzed using the CPPTRAJ module. The ADME properties are predicted using QikProp from Schrodinger Schrödinger Release 2019-1: QikProp, Schrödinger, LLC, New York, NY, 2019.

Thermal shift assay.[67] In brief, the test compounds were added to the wells containing protein and fluorescent dye, and ligand-induced alteration in thermal stability was measured (n = 3) by monitoring the fluorescence while heating the samples from 25 °C to 95 °C in small intervals. The thermal shift assay is based on the principle that when the ligand binds to a protein, the ligand mostly stabilizes the protein and the melting temperature (T_m) of the ligand-protein complex is different than that of the unbound protein. For a typical experiment, the huCOX-2 or muCOX-1 (Cayman Chemical, Ann Arbor, USA) was taken in a microtiter plate (1μM in 25mM Tris pH 8.0), and the test compounds were added to the protein (final concentration = 50 μM) and incubated on ice for 30 minutes. Thiol-reactive fluorescent dye 7-diethyl-amino-3-(4'-maleimidy-lphenyl)-4-methylcoumarin (CPM, final concentration = 50 μM) was added to each well. For inducing thermal unfolding of the protein, the temperature was increased from 25 °C to 95 °C (0.5 °C increments) over the 40 min, and the change in fluorescence emission was monitored. The difference in melting temperature (ΔT_M) calculated by comparing melting temperature (Tm) curves of ligand-bound protein and unbound protein. All the experiments performed in triplicate, and celecoxib **1**, a clinically used selective COX-2 inhibitor, was used as a positive control in all experiments.

Cell culture and fluorescence imaging. The human colon cancer cell line, HCA-7 colony 29 cells (Sigma Aldrich, 02091238) used for fluorescence imaging of COX-2 over-expression. For a comparison, COX-2 negative, HCT-116 cells (ATCC) were used. The COX-2 protein expression in and HCA-7 and HCT-116 cells was determined, by following our standard Western blotting analysis procedure.[68] An immunostaining experiment using anti-COX-2 mouse monoclonal antibody was performed to confirm the perinuclear COX-2 expression.[69] For imaging studies in HCA-7 cells, the cells were cultured in T75 flasks using DMEM/F12 (1:1) medium supplemented with 10% (v/v) fetal bovine serum (FBS, GIBCO, 12483), 2 mM L-glutamine (GIBCO, 25030), 1% penicillin/streptomycin and 20 mM HEPES buffer (GIBCO, 15630) and were kept in a 37 °C humidified incubator with a supply of 5% CO_2 in air. After the cells were 80% confluent, they were harvested using 0.25% trypsin-EDTA (GIBCO, 25200) and plated onto sterile glass-bottom dishes (pre-equilibrated culture medium at 37 °C) at a density of 200,000 cells/well, incubated for 24 hours. On the day of fluorescence imaging cells were incubated with click chemistry precursor compound **14** (0.1% DMSO in growth media), a series of experiments were performed for each test compound by varying incubation time (1 to 30 min) and concentration (0.1 to 100 μM). The cells were then washed with 3 x 400 μL PBS, then incubated with 100 μL freshly prepared biocompatible click chemistry reagent solution (BTTPS/Cu^I) and compound **11** (0.1 to 100 μM, 0.1% DMSO in growth media). Fresh click chemistry reagent solution was prepared by premixing 0.5 μL $CuSO_4$ (50 mM) in H_2O and 3 μL BTTPS (50 mM) in H_2O to PBS (481.5 μL), then after 12.5 μL freshly prepared sodium ascorbate (100 mM in PBS) was added. The click chemistry solution was comprised of 50 μM $CuSO_4$, 300 μM BTTPS, 2.5 mM sodium ascorbate in PBS. Followed by the incubation in 5% CO_2 atmosphere at 37 °C for different time intervals (1-30 min), the cells were washed with PBS buffer and the supernatant was discarded, and the cells were fixed with 2% paraformaldehyde in PBS, and nuclei were stained with DAPI (50 µg mL^{-1}) and imaged with a confocal laser scanning microscope.

For live-cell imaging, nuclei were stained with Hoechst 33258, for plasma membrane staining CellMask Deep red was added to the dishes, the cells were imaged in a warm (37 °C), 5% CO_2 in air flow, humidified imaging chamber equipped with a microscope. The cells were imaged using corresponding lasers for visualizing DAPI (blue nuclear staining), and FITC (green emission) with a Plan- Apochromat 40X/1.3 Oil DIC M27 lens on a Zeiss LSM 710 AxioObserver confocal laser scanning microscope. All treatments performed in duplicate dishes in at least three separate experiments. *COX-2 active site blocking studies*: The cells were pre-incubated with celecoxib **1** (1-100 μM) for 15 min before the addition of the other click chemistry compounds to block the COX-2 active site.

For real-time imaging of Cu-free click chemistry reaction in live HCA-7 cells, clear glass bottom dishes were placed on the microscope platform, and collection of cells were focused. Sequence wise celecoxib-azide **14** (0.1 to 100 μM, 0.1% DMSO in growth media) was incubated for 5 min, followed by NBD-DBCO **17** (0.1 to 100 μM, 0.1% DMSO in growth media) and incubated at 37 °C, washed gently with media, followed by the addition of Hoechst 33258 nuclear stain, CellMask Deep red plasma membrane stain. Throughout the experiment, to guarantee live cell conditions, a chamber box with a microscope was incubated at 37 °C, humidified, with 5% CO2 containing airflow. Live-cell confocal images were collected at regular intervals, as well as in a separate experiment *in cellulo* generation of fluorescent imaging probe was also recorded (Supplementary movie) while maintaining the focus of microscope on the same collection of cells.

HCT-116 cells: HCT-116 cells (ATCC), COX-2 negative, were used for confirming the role of COX-2 *in cellulo* generation of COX-2 imaging probes. HCT-116 cells were cultured at 37 °C in a humidified atmosphere of 5% CO2 (v/v), using DMEM/F12 (1:1) medium supplemented with 10% FBS (GIBCO, 25030), 2 mM L-

glutamine (GIBCO, 25030), and 1% antibiotic/antimycotic (Invitrogen). The cell growth medium changed every other day. After the cells were 80% confluent, the cells were treated with 0.25% trypsin-EDTA (1mM, GIBCO, 25200) for ~5 min at room temperature to dissociate cells from the culture flask and rinsed with PBS once after harvesting. Cells were plated onto sterile glass-bottom dishes (pre-equilibrated culture medium at 37 °C) at a density of 200,000 cells/well. Cells on coverslips were allowed to incubate for an additional 24 hours. All other studies with click chemistry precursors and reagents were performed by following the above described procedure.

Acknowledgments

We gratefully acknowledge the Dianne and Irving Kipnes Foundation, the Canadian Institute for Health Research (CIHR) and the National Science and Engineering Research Council of Canada (NSERC) for supporting this work. F.W. and J.K. thank the Alberta Cancer Foundation (ACF) for a postdoctoral fellowship. We thank Prof. Edward E. Knaus, for his valuable suggestions throughout this study, Alison Marshall, for help with cell culture work, and Vishwa Somayaji, for his help with LC/MS analyses.

Author contributions: A.B. and J.K. contributed equally to this research work. A.B. and J.K. performed computational analyses. A.B. and J.K. synthesized the compounds. A.B. designed and performed fluorescence and LC/MS analyses, TSA experiments, stability analyses. J.K. performed in vitro and cellular biological experiments. A.B. and J.K. designed and performed fluorescence imaging experiments. A.B. and J.K. wrote manuscript and compiled the supporting information. A.B., J.K., and F.W. analyzed the data, discussed the results, and contributed to the editing of the manuscript.

Conflict of interest: The authors declare no competing financial interests.

Keywords: Imaging agents • Fluorescence • Cyclooxygenase • Drug Design • Cancer

References:

[1] M. A. Miller, R. Weissleder, *Nat. Rev. Cancer.* **2017**, *17*, 399-414.

[2] M. Koch, V. Ntziachristos, *Annu. Rev. Med.* **2016**, *67*, 153-164.

[3] J. K. Willmann, N. van Bruggen, L. M. Dinkelborg, S. S. Gambhir, *Nat. Rev. Drug Discov.* **2008**, *7*, 591-607.

[4] W. L. Smith, Y. Urade, P. J. Jakobsson, *Chem. Rev.* **2011,** *111*, 5821-5865.

[5] D. Wang, R. N. DuBois, *Nat. Rev. Cancer.* **2010**, *10*, 181-193.

[6] J.-B. Meric, S. Rottey, K. Olaussen, J.-C. Soria, D. Khayat, O. Rixe, J.-P. Spano, *Crit. Rev. Oncol. Hematol.* **2006**, *59*, 51-64.

[7] L. Xu, J. Stevens, M. B. Hilton, S. Seaman, T. P. Conrads, T. D. Veenstra, D. Logsdon, H. Morris, D. A. Swing, N. L. Patel, J. Kalen, D. C. Haines, E. Zudaire, B. St. Croix, *Sci. Transl. Med.* **2014**, *6*, 1-8.

[8] R. E. Harris, *Inflammopharmacology*, **2009**, *17*, 55-67.

[9] M. D. Castellone, H. Teramoto, B. O. Williams, K. M. Druey, J. S. Gutkind, *Science,* **2005**, *310*, 1504-1510.

[10] C. M. Ulrich, J. Bigler, J. D. Potter, *Nat. Rev. Cancer,* **2006**, *6*, 130-140.

[11] M. M. Bertagnolli, C. J. Eagle, A. G. Zauber, M. Redston, S. D. Solomon, K. Kim, J. Tang, R. B. Rosenstein, J. Wittes, D. Corle, T. M. Hess, G. M. Woloj, F. Boisserie, W. F. Anderson, J. L. Viner, D. Bagheri, J. Burn, D. C. Chung, T. Dewar, T. R. Foley, N. Hoffman, F. Macrae, R. E. Pruitt, J. R. Saltzman, B. Salzberg, T. Sylwestrowicz, G. B. Gordon, E. T. Hawk, *N. Engl. J. Med.* **2006**, *355*, 873-84.

[12] Y. I. Cha, R. N. DuBois, *Annu Rev Med*. **2007**, *58*, 239-52.

[13] M. J. Uddin, B. C. Crews, A. L. Blobaum, P. J. Kingsley, L. Gorden, O. McIntyre, L. M. Matrisian, K. Subbaramaiah, A. J. Dannenberg, D. W. Piston, L. J. Marnett, *Cancer Res.* **2010**, *70*, 3618-3627.

[14] H. Zhang, J. Fan, J. Wang, B. Dou, F. Zhou, J. Cao, J. Qu, Z. Cao, W. Zhao, X. Peng, *J. Am. Chem. Soc.* **2013**, *135*, 17469-17475.

[15] M. J. Uddin, B. C. Crews, K. Ghebreselasie, L J. Marnett, *ACS Med. Chem. Lett.* **2011**, *2*, 160-164.

[16] A. Bhardwaj, J. Kaur, S. K. Sharma, Z. Huang, F. Wuest, E.E. Knaus, *Bioorg. Med. Chem. Lett.* **2013**, *23*,163-168.

[17] J. Kaur, O. Tietz, A. Bhardwaj, A. Marshall, J. Way, M. Wuest, F. Wuest, *ChemMedChem*, **2015**, *10*, 1635-1640.

[18] M. Laube, T. Kniess, J. Pietzsch, *Molecules,* **2013**, *18*, 6311-6355.

[19] A. Morgenroth, A. T. J. Vogg, B. Neumaier, F. M. Mottaghy, B. D. Zlatopolskiy, *Oncotarget*, **2017**, *8*, 18059-18069.

[20] A. L. Blobaum, L. J. Marnett, *J. Med. Chem.* **2007**, *50*, 1425-1441.

[21] R. G. Kurumbail, A. M. Stevens, J. K. Gierse, J. J. McDonald, R. A. Stegeman, J. Y. Pak, D. Gildehaus, J. M. iyashiro, T. D. Penning, K. Seibert, P. C. Isakson, W. C. Stallings, *Nature*, **1996**, *384*, 644-648.

[22] H. C., Kolb, M. G. Finn, K. B. Sharpless, *Angew. Chem. Int. Ed.* **2001**, *40*, 2004-2021.

[23] V. V. Rostovtsev, L. G. Green, V. V. Fokin, K. B. Sharpless, *Angew. Chem., Int. Ed.* **2002**, *41*, 2596-2599.

[24] E. Haldón, M. C. Nicasio, P. J. Pérez, *Org. Biomol. Chem.* **2015**, *13*, 9528-9550.

[25] P. Thirumurugan, D. Matosiuk, K. Jozwiak, *Chem. Rev.* **2013**, *113*, 4905-4979.

[26] W. G. Lewis, L. G. Green, F. Grynszpan, Z. Radić, P. R. Carlier, P. Taylor, M. G. Finn, K. B. Sharpless, *Angew. Chem. Int. Ed.* **2002**, *41*, 1053-1101.

[27] Z. Liu, J. Li, S. Li, G. Li, K. B. Sharpless, P. Wu, *J. Am. Chem. Soc.* **2018**, *140*, 2919-2925.

[28] N. J. Agard, J. A. Prescher, C. R. Bertozzi, *J. Am. Chem. Soc.* **2004**, *126*, 15046-15047.

[29] H., Wu, N. K. Devaraj, *Acc. Chem. Res.* **2018**, *51*, 1249-1259.

[30] N. K., Devaraj, R. Upadhyay, J. B. Haun, S. A. Hilderbrand, R. Weissleder, *Angew Chem. Int. Ed. Engl.* **2009**, *48*, 7013-7016.

[31] J. C. Jewett, C. R. Bertozzi, *Chem. Soc. Rev.* **2010**, *39*, 1272-1279.

[32] J. Dong, L. Krasnova, M. G. Finn, K. B. Sharpless, *Angew Chem. Int. Ed. Engl.* **2014**, *53*, 9430-9448.

[33] R. Manetsch, A. Krasiński, Z. Radić, J. Raushel, P. Taylor, K. B. Sharpless, H. C. Kolb, *J. Am. Chem. Soc.* **2004**, *126*, 12809-12818.

[34] N. P. Grimster, B. Stump, J. R. Fotsing, T. Weide, T. T. Talley, J. G. Yamauchi, Á. Nemecz, C. Kim, K.-Y. Ho, K. B. Sharpless, P. Taylor, V. V. Fokin, *J. Am. Chem. Soc.* **2012**, *134*, 6732-6740.

[35] S. G. Rzuczek, H. Park, M. D. Disney, *Angew. Chem. Int. Ed.* **2014**, *53*,10956-10959.

[36] I. Glassford, C. N. Teijaro, S. S. Daher, A. Weil, M. C. Small, S. K. Redhu, D. J. Colussi, M. A. Jacobson, W. E. Childers, B. Buttaro, A. W. Nicholson, A. D. Mackerell Jr., B. S. Cooperman, R. B. Andrade, *J. Am. Chem. Soc.* **2016**, *138*, 3136-3144.

[37] A. Bhardwaj, J. Kaur, M. Wuest, F. Wuest, *Nat. Commun.* **2017**, *8*, 1-13.

[38] A. Saghatelian, N. Jessani, A. Joseph, M. Humphrey, B. F. Cravatt, *Proc. Natl. Acad. Sci. USA* **2004**, *101*, 10000-10005.

[39] L. I. Willems, W. A. Van Der Linden, N. Li, K.-Y. Li, N. Liu, S. Hoogendoorn, G. A. van der Marel, B.I. Florea, H. S. Overkleeft, *Acc. Chem. Res.* **2011**, *44*, 718-729.

[40] K. S. Yang, G. Budin, C. Tassa, O. Kister, R. Weissleder, *Angew. Chem. Int. Ed.* **2013**, *52*, 10593-10597.

[41] C. D. Spicer, B. G. Davis, *Nat. Commun.* **2014**, *5*, 4740-4753.
[42] J. A. Prescher, D. H. Dube, C. R. Bertozzi, *Nature* **2004**, *430*, 873-877.
[43] M. Sawa, T.-L. Hsu, T. Itoh, M. Sugiyama, S. R. Hanson, P. K. Vogt, C.-H. Wong, *Proc. Natl. Acad. Sci. U. S. A.* **2006**, *103*, 12371-12376.
[44] S. T. Laughlin, J. M. Baskin, S. L. Amacher, C. R. Bertozzi, *Science,* **2008**, *320*, 664-667.
[45] S. H. Rouhanifard, L. U. Nordstrøm, T. Zheng, P. Wu, *Chem. Soc. Rev.* 2013, *42*, 4284-4296.
[46] J. T. Ngo, B. M. Babin, J. A. Champion, E. M. Schuman, D. A. Tirrell, *Nat. Chem. Biol.* **2009**, *5*, 715-717.
[47] D. K. Nomura, M. M. Dix, B. F. Cravatt, *Nat. Rev. Cancer.* **2010**, *10*, 630-638.
[48] H. Wu, N. K. Devaraj, *Acc. Chem. Res.* **2018**, *51*, 1249-1259.
[49] K. S. Yang, G. Budin, T. Reiner, C. Vinegoni, R. Weissleder, *Angew. Chem. Int. Ed.* **2012**, *51*, 6598-6603.
[50] N. K. Devaraj, S. Hilderbrand, R. Upadhyay, R. Mazitschek, R. Weissleder, *Angew. Chem., Int. Ed.* **2010**, *49*, 2869-2872.
[51] A. B. Neef, C. Schultz, *Angew. Chem. Int. Ed.* **2009**, *48*, 1498-1500.
[52] C. Y. Jao, M. Roth, R. Welti, A. Salic, *Proc. Natl. Acad. Sci. USA* **2009**, *106*, 15332-15337.
[53] A. B. Neef, N. W. Luedtke, *Proc. Natl. Acad. Sci. USA.* **2011**, *108*, 20404-20409.
[54] A. H. El-Sagheer, T. Brown, *Acc. Chem. Res.* **2012**, *45*, 1258-1267.
[55] K. Nguyen, M., M. F. Kubota, S. Nainar, C. Feng, X. Li, S. X. Atwood, T. W. Bredy, R. C. Spitale, *J. Am. Chem. Soc.* **2017**, *139*, 2148-2151.
[56] D. Ye, A. J. Shuhendler, L. Cui, L. Tong, S. S. Tee, G. Tikhomirov, D. W. Felsher, J. Rao, *Nat. Chem.* **2014**, ***6***, 519-526.
[57] M. Yang, A. S. Jalloh, W. Wei, J. Zhao, P. Wu, P. R. Chen, *Nat. Commun.* **2014**, *5*, 4981-4990.
[58] N. Arber, C. J. Eagle, J. Spicak, I. Rácz, P. Dite, J. Hajer, M. Zavoral, M. J. Lechuga, P. Gerletti, J. Tang, R. B. Rosenstein, K. Macdonald, P. Bhadra, R. Fowler, J. Wittes, A. G. Zauber, S. D. Solomon, B. Levin, *N. Engl. J. Med.* **2006,** *355*, 885-895.
[59] N. S. Kirkby, M. H. Lundberg, L. S. Harrington, P. D. M. Leadbeater, G. L. Milne, C. M. F. Potter, M. A.-Yamani, O. Adeyemi, T. D. Warner, J. A. Mitchell, *Proc. Natl. Acad. Sci. USA* **2012**, *109*, 17597-17602.
[60] W. Wang, S. Hong, A. Tran, H. Jiang, R. Triano, Y. Liu, X. Chen, P. Wu, *Chem. Asian J.* **2011**, *6*, 2796-2802.
[61] K. Sivakumar, F. Xie, B. M. Cash, S. Long, H. N. Barnhill, Q. Wang, *Org. Lett.* **2004**, *6*, 4603-4606.
[62] G. Zhou, H. Wang, Y. Ma, X. Chen. *Tetrahedron.* **2013**, *69*, 867-870.
[63] W. Phetsang, M. A. Blaskovich, M. S. Butler, J. X. Huang, J. Zuegg, S. K. Mamidyala, S. Ramu, A. M. Kavanagh, M. A. Cooper, *Bioorg. Med. Chem*. **2014**, *22*, 4490-4498.
[64] G. A. Crosby, J. N. Demas, *Chem. Rev*. **1971**, *75*, 991-1024.
[65] J. W. Ponder, D. A. Case, *Adv. Prot. Chem*. **2003**, *66*, 27-85.
[66] J. A. Maier, K. Kasavajhala, L. Wickstrom, K. E. Hauser, C. Simmerling, *J. Chem. Theory Comput.* **2015**, *11*, 3696-3713.
[67] L. Dong, C. Yuan, B. J. Orlando, M. G. Malkowski, W. L. Smith, *J. Biol. Chem.* **2016**, *291*, 25641-25655.
[68] O. Tietz, M. Wuest, A. Marshall, D. Glubrecht, I. Hamann, M. Wang, C. Bergman, J. Way, F. Wuest, *EJNMMI Res*. **2016**, *6*, 37.
[69] A. Bhardwaj, J. Kaur, S. Sharma, Z. Huang, F. Wuest, E. E. Knaus. *Bioorg. Med. Chem. Lett.* **2013**, *23*, 163-168.

10.1002/chem.202003315

WILEY-VCH

FULL PAPER

Graphical abstract

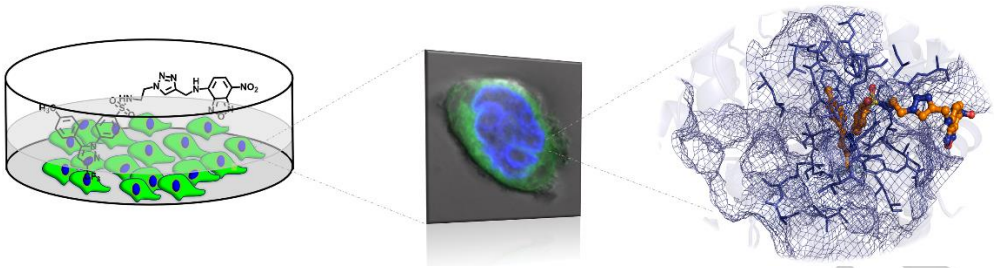

In cellulo click chemistry to generate highly fluorescent COX-2 imaging probes in living cells